

# ROSE optical memory protocol in the waveguide of a Tm:YAG crystal

© M.M. Minnegaliev<sup>1</sup>, A.V. Pavlov<sup>1</sup>, K.I. Gersimov<sup>1</sup>, E.S. Moiseev<sup>1</sup>, N.N. Skryabin<sup>2</sup>,  
A.A. Kalinkin<sup>2</sup>, S.P. Kulik<sup>2,3</sup>, S.A. Moiseev<sup>1</sup>

<sup>1</sup>Kazan Quantum Center, Kazan National Research Technical University named after A.N. Tupolev, 420111 Kazan, Russia

<sup>2</sup>Centre for Quantum Technologies, Department of Physics, Lomonosov Moscow State University, 119991 Moscow, Russia

<sup>3</sup>Laboratory „Quantum Engineering of Light“, South Ural State University, 454080 Chelyabinsk, Russia

e-mail: mansur@kazanqc.org

Received November 09, 2023

Revised January 20, 2023

Accepted March 23, 2023.

In this work, optical spectroscopy of thulium ions in a single-mode optical waveguide fabricated in a  $\text{Tm}^{3+}:\text{Y}_3\text{Al}_5\text{O}_{12}$  crystal using the femtosecond laser printing method was carried out and an optical quantum memory protocol was demonstrated in a revival of silenced echo scheme. An analysis of the experimental data indicates the presence of instantaneous spectral diffusion at a thulium ion concentration of less than 0.01%, a weak effect of imperfections in the formed waveguide on the lifetime of the optical memory, and indicates the possibility of achieving a high efficiency of input signal recovery in the implemented waveguide scheme of the protocol.

**Keywords:** rare-earth ions, photon echo, optical quantum memory, ROSE, femtosecond laser printing.

DOI: 10.61011/EOS.2023.05.56512.74-22

## 1. Introduction

Recent advances in integrated quantum photonics [1] have accelerated the development of optical quantum memory (QM) in integrated form, which is used in the implementation of various quantum technologies, such as quantum communication over long distances [2], preparation of the initial quantum state [3], synchronization for optical quantum processing [4] and many others. Waveguides fabricated by femtosecond laser printing in crystals doped with rare-earth ions (REI) can serve as a convenient platform for such integrated quantum memory. REI-doped crystals can potentially be used for multiplexing and long-term storage of signals due to the unique combination of narrow homogeneous and large inhomogeneous broadening of optical transitions. Moreover, fabricating multiple waveguides on a single crystal can provide additional spatial multiplexing. Recently, optical memory in such waveguides was realized in papers [5,6]. Quantum memory in REI-activated waveguides has been demonstrated for single photons [7], photonic qubits [8] and using frequency multiplexing [9].

Most of the above experiments use the atomic frequency comb (AFC) protocol [10], in which a photonic qubit is written into the collective atomic coherence of an atomic ensemble with an equidistant spectrum. As a result of interference of equidistant individual frequency peaks, the system emits an absorbed signal in the form of an optical echo at time  $2\pi/\Delta$ , where  $\Delta$  — the distance between individual spectrum peaks. The storage time of this protocol is often limited by the minimum achievable parameter  $\Delta$ , which is usually in the range from 0.1 to 1 MHz. This results in a storage time on the order of microseconds, which may not be sufficient for practical applications [4]. A longer

storage time requires the transfer of coherence from the optical transition to a long-lived spin sublevel. This can be done using an additional  $\pi$  pulse, as was done for bright input light pulses in femtosecond laser printed waveguides in  $^{151}\text{Eu}^{3+}:\text{Y}_2\text{SiO}_5$  crystal [6]. In addition, in such a waveguide in the  $^{151}\text{Eu}^{3+}:\text{Y}_2\text{SiO}_5$  crystal, the optical QM protocol was implemented in the revival of silenced echo (ROSE) scheme [6,11–13]. This scheme has several advantages. First, this protocol allows to use the natural inhomogeneous broadening of the atomic transition and does not require an additional step of spectrum preparation in the form of AFC. Second, the QM storage time in the ROSE scheme mainly depends on the atomic transition coherence time. Thirdly, the extraction of the stored light can be realized with just two rephasing  $\pi$  pulses. As a consequence, longer storage times and on-demand retrieval are easier to achieve with the ROSE protocol. However, the experimental implementation of high quality  $\pi$  pulses is still an extremely difficult task.

In the present paper, a waveguide of the third type was fabricated by femtosecond laser printing. The advantage of such waveguide structures is that radiation with arbitrary light polarization can propagate in them [14,15]. Next, stationary and coherent optical spectroscopy of the formed waveguide structure and the bulk part of the crystal was carried out. The ROSE protocol was experimentally implemented in the fabricated waveguide. In conclusion, ways to increase the efficiency of the input signal reduction and increase the storage time are discussed.

## 2. Experimental setup

As a radiation source, we used a Tekhnoscan TIS-SF-777 cw narrow-band titanium-sapphire laser. The laser

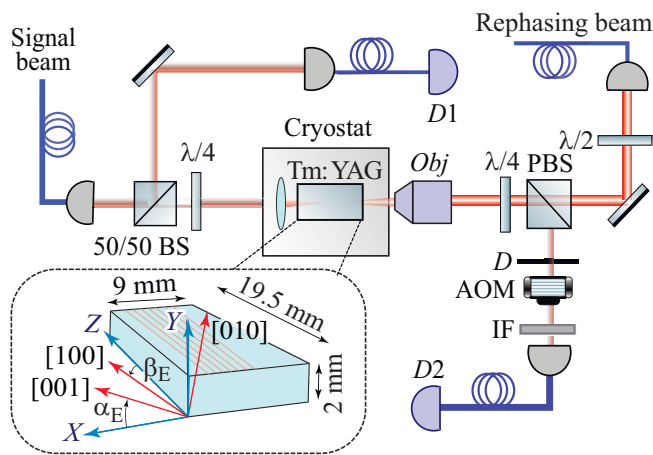


**Figure 1.** A simplified sketch of the experimental setup, where *BS* — beam splitter, *PBS* — polarization beam splitter, *D* — iris diaphragm, *IF* — interference filter, *D1/D2* — detectors. Insert: orientation of the crystallographic axes of a Tm:YAG crystal relative to its faces.

was tuned to the transition  ${}^3\text{H}_6(0) \rightarrow {}^3\text{H}_4(0)$  of  $\text{Tm}^{3+}$  ( $\lambda \approx 793.365$  nm) ions in the  $\text{Y}_3\text{Al}_5\text{O}_{12}$  (YAG) crystal. Two acousto-optic modulators (AOM) are used to form pulses to generate a two-pulse echo and implement the ROSE protocol. After passing through the AOM, the radiation passes through a single-mode fiber for spatial filtering of the light mode. The formed signal light pulse propagates along the *Z* axis parallel to the long edge of the crystal (19.5 mm), and the rephasing pulses — in the opposite direction to it at a small angle  $\beta_E = 4.3^\circ$  with respect to the crystallographic axis  $[100]$  (insert in Fig. 1). The crystallographic axes of the crystal are oriented with respect to the crystal faces, as shown in the inset in Fig. 1, where  $\alpha_E = 11.3^\circ$ ,  $\beta_E = 4.3^\circ$ ,  $\gamma_E = 0^\circ$  are the Euler angles. The signal and rephasing beams were circularly polarized in front of the crystal.

The simplified experimental setup after leaving the fibers is shown in Fig. 1. The rephasing beam is launched into the waveguide by an objective (Edmund Optics ELWD 10x 59877) on one side of the crystal, and the signal beam — using an aspherical lens (Thorlabs A280TM-B) installed in the cryostat on the other side of the crystal. A Tm:YAG crystal with a concentration of  $c = 0.01\%$  and dimensions of  $2 \times 9 \times 19.5$  mm is placed in a closed-cycled cryostat (Montana Instruments Corp.). The crystal was glued to the cold finger of the cryostat, which was cooled to a temperature of  $T = 3.2 \pm 0.1$  K. In a crystal, 21 type III waveguides with different diameters were fabricated parallel to the *Z* axis. Each waveguide was made by burning 18 elliptical depressed regions of the shell with axes 2 and  $8 \mu\text{m}$  along a circle with a diameter of  $18 \mu\text{m}$  using a femtosecond laser. The fabricated waveguide has a Gaussian mode with a half-width at half-maximum  $\sim 5.5 \mu\text{m}$  on both axes.

### 3. Spectroscopy of the waveguide

First, we carried out stationary and coherent optical spectroscopy of the bulk part of the crystal and the waveguide. In this case, a single-mode waveguide was chosen with the following parameters: diameter  $18 \mu\text{m}$ , propagation loss for vertical polarization of light (parallel to side 2 mm of the crystal) 0.66 dB/cm, for horizontal polarization of light (parallel to side 9 mm) 1.13 dB/cm. To determine the transverse spatial structure of the light mode, the fundamental mode in this waveguide was calculated by the finite element method. The difference in refractive indices  $\Delta n$  between the crystal areas treated with a femtosecond laser and untreated was estimated in the range  $1 \cdot 10^{-4} - 8 \cdot 10^{-3}$ . For these parameters, the fundamental mode has a Gaussian form with transverse half-widths  $\sigma \sim 5.1 \mu\text{m}$ . Spectroscopic studies of the waveguide in a Tm:YAG crystal were obtained using the laser signal beam shown in Fig. 1. The absorption at the optical transition for the bulk crystal and waveguide was  $\alpha L = 0.26$  and  $\alpha L = 0.12 \pm 0.04$ , respectively, where  $L = 19.5$  mm. Thus, the value of the absorption coefficient was  $\alpha_0 = 0.06 \text{ cm}^{-1}$  for the waveguide part and  $\alpha_0 = 0.14 \text{ cm}^{-1}$  at the line maximum for the bulk crystal. The latter correlates with the values of the absorption coefficient  $\alpha_0 = 1 \text{ cm}^{-1}$  (concentration 0.05%) and  $\alpha_0 = 2.3 \text{ cm}^{-1}$  (concentration 0.1%), measured respectively in [16] and [17]. It should be noted that the inhomogeneous broadening of the optical transition line increased for the waveguide part, which amounted to  $\Gamma_{\text{inh}} = 30 \pm 3$  GHz, compared with  $\Gamma_{\text{inh}} = 10.5$  GHz for the bulk part of the crystal. The center frequency of the optical transition absorption peak has shifted by approximately 10 GHz ( $\nu = 378.130$  THz for a bulk crystal and  $\nu = 378.140$  THz for a waveguide). The absorption spectra are shown in Fig. 2, *a*.

Approximation of the decrease in the intensity of a two-pulse photon echo depending on the time delay between excitation pulses  $\tau$  according to the Mims formula,  $I = I_0 e^{-2(\frac{\tau}{T_M})^x}$  allowed to determine the coherence time  $T_M = 72.2 \mu\text{s}$  ( $x = 1.55$ ) for the bulk part of the crystal and  $T_M = 63 \mu\text{s}$  ( $x = 1.82$ ) for the waveguide (Fig. 2, *b*). All parameters measured in this section are given in the table.

### 4. Implementation of the ROSE protocol in the waveguide

The ROSE quantum memory protocol was implemented in this waveguide. Fig. 1 shows the path of the signal beam along which the input pulse propagated. The signal and rephasing beams were circularly polarized in front of the crystal. Fig. 3 shows experimental data on the optical storage of a weak input light pulse obtained using the ROSE protocol in a waveguide. The signal pulse (black curve) had a Gaussian time form with a duration of  $1 \mu\text{s}$  (full width at

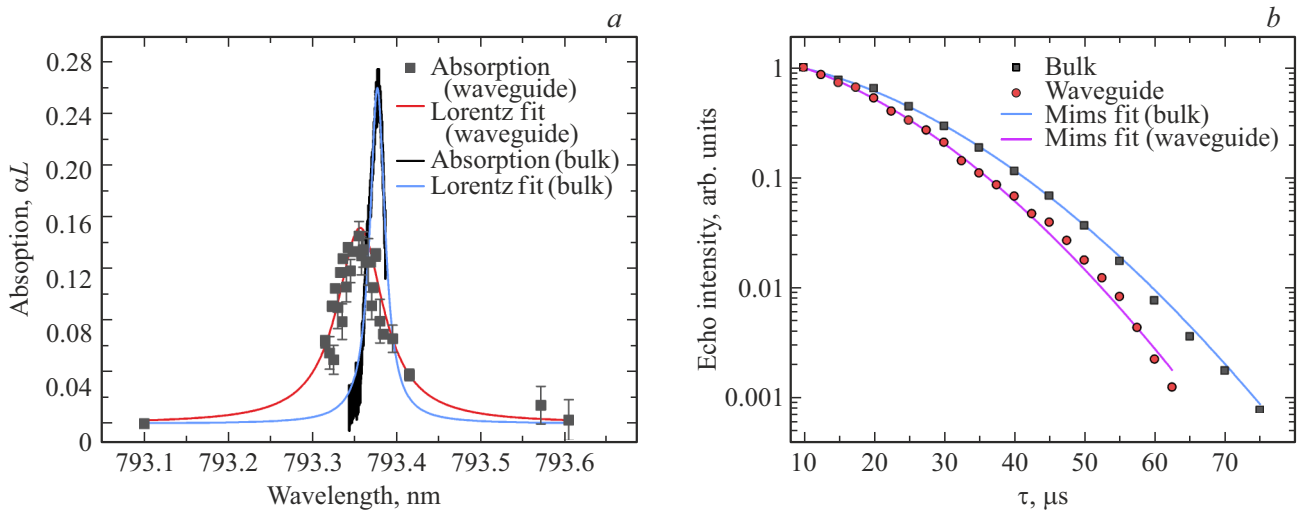


**Figure 2.** Experimental results on optical spectroscopy of the  ${}^3H_6(0) \rightarrow {}^3H_4(0)$  transition of thulium ions in  $Tm^{3+}:Y_3Al_5O_{12}$  ( $c = 0.01\%$ ) crystal at a temperature of  $T = 3.2 \pm 0.1$  K. (a) Absorption spectrum for the bulk part (solid black line) and in the waveguide (black squares); the Lorentz function approximation is shown by the blue and red solid curves. (b) Dependence of the two-pulse echo signal intensity on a logarithmic scale on the delay time between pulses  $\tau$  for the bulk part of the crystal (black squares) and the waveguide (red circles); solid lines correspond to the approximation of the experimental results by the Mims formula.

Spectroscopic parameters of thulium ions in  $Tm^{3+}:Y_3Al_5O_{12}$  ( $c = 0.01\%$ ) crystal at the  ${}^3H_6(0) \rightarrow {}^3H_4(0)$  optical transition, measured in the bulk part of the crystal and in the waveguide at  $T = 3.2 \pm 0.1$  K

	Bulk crystal	Waveguide
Absorption $\alpha L$	0.266	$0.12 \pm 0.04$
Value of inhomogeneous broadening	10.5 GHz	$30 \pm 3$ GHz
Central frequency of the transition	378.130 THz	378.140 THz
Coherence time	$T_M = 72.2 \mu s$ ( $x = 1.55$ )	$T_M = 63 \mu s$ ( $x = 1.82$ )

half-maximum). The red curve shows the unabsorbed part of the input pulse. Rephasing pulses at times  $t = 7.5 \mu s$  and  $t = 22.5 \mu s$  are shown in blue. As rephasing  $\pi$  pulses, we used laser pulses with amplitude and frequency modulation. The amplitude of the electric field  $\varepsilon(t)$  and the carrier frequency  $\omega(t)$  of pulses were set in the following form:

$$\varepsilon(t) = \varepsilon_0 \operatorname{sech}(\beta(t - t_0)),$$

$$\omega(t) = \omega_0 + \mu\beta \tanh(\beta(t - t_0)),$$

where the parameters  $\beta$  and  $\mu$ , which determine the pulse duration ( $\beta^{-1}$ ) and its spectral width ( $2\mu\beta$ ), were set and controlled experimentally. Such pulses allow to effectively

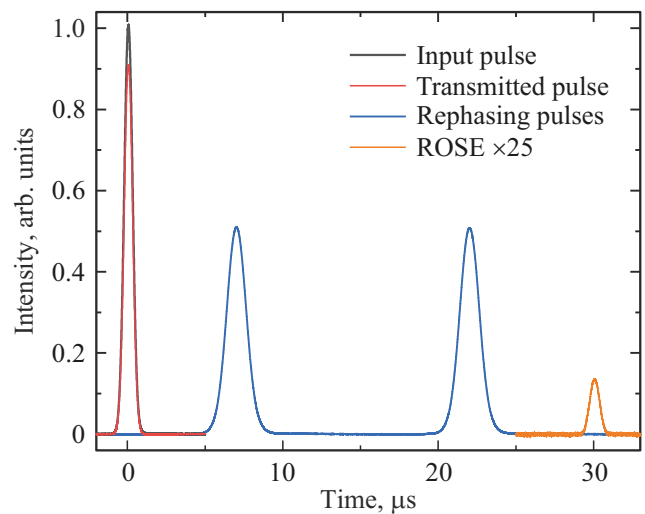


**Figure 3.** Revival of silenced echo signal in a waveguide in a crystal  $Tm^{3+}:Y_3Al_5O_{12}$  at  $t = 30 \mu s$  (ROSE, orange curve) with a magnification of 25 times. Rephasing pulses are shown in blue. The input pulse ( $t = 0 \mu s$ ) and its unabsorbed part are shown in black and red, respectively.

invert the Bloch vector of atoms the resonant frequencies of which lie in the limit of the spectral interval  $2\mu\beta$  under the adiabaticity condition for the evolution of the Bloch vector  $\mu\beta^2 \ll \Omega_{1,2}^2$  and in the presence of a rather weak damping of atomic coherence,  $T_M\beta \gg 1$ . In our experiments, the parameters of laser pulses were varied in the range of  $\beta = 2\pi \times (140 - 400)$  kHz and  $\mu = 1 - 4$  so that the spectral interval of the control pulse frequency sweep overlapped the spectrum of the signal light fields. The input

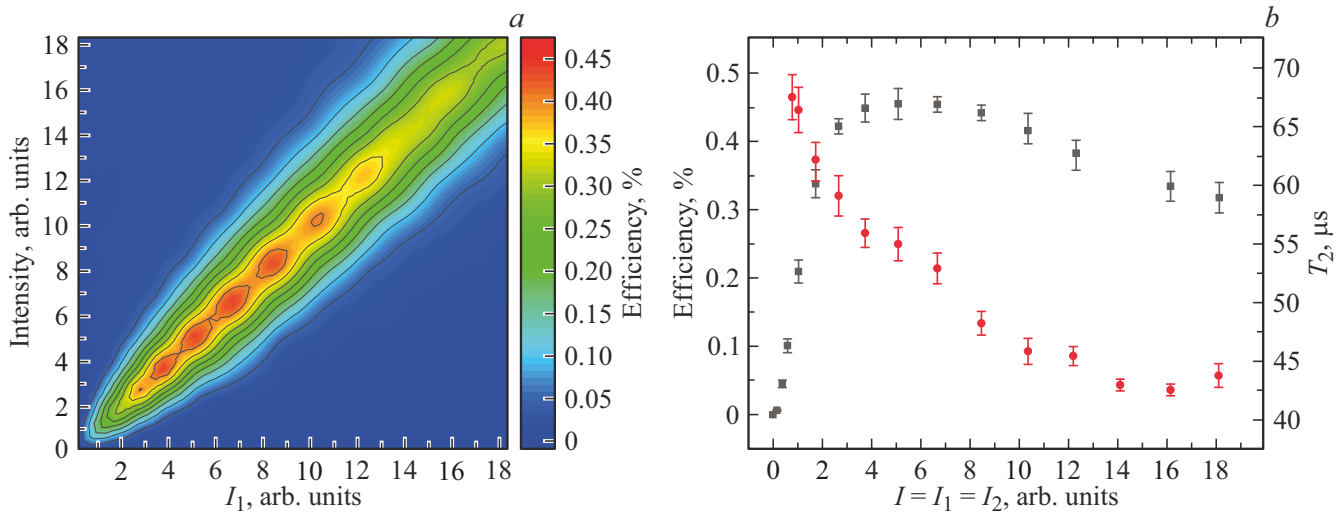


**Figure 4.** (a) The results of measuring the recovery efficiency of the input pulse in the waveguide optical memory depending on the intensity of the first  $I_1$  and second  $I_2$  rephasing pulses. (b) Input pulse recovery efficiency (black squares) and optical transition coherence time  $T_2$  measured using the ROSE sequence (red circles) in a waveguide optical memory as a function of the intensity of rephasing pulses at  $I = I_1 = I_2$ .

pulse was measured on the detector D1, the unabsorbed part of the input pulse and the signal ROSE — on a similar detector D2 (Fig. 1). The  $\eta$  (recovery efficiency) is defined as the ratio of the echo signal intensity to the input pulse intensity and was 0.5% for a storage time of  $30\mu\text{s}$ . It should be noted that for the propagation geometry of the signal and rephasing pulses used, as well as the absorption value  $\alpha L = 0.12$  and the coherence time of the optical transition  $T_M = 63\mu\text{s}$  ( $x = 1.82$ ), the maximum achievable efficiency is  $\eta_{\text{max}} = 0.76\%$ . This estimate was obtained according to the formula  $\eta_{\text{max}} = \alpha L^2 e^{-\alpha L} e^{-2\left(\frac{2\tau}{T_M}\right)^x}$ , where  $2\tau$  — storage time. The signal recovery efficiency can be noticeably increased by using a crystal with a higher absorbance and optical transition coherence time, for example, in the  $^{167}\text{Er}^{3+}:\text{Y}_2\text{SiO}_5$  [13,18] crystal. The optical transition of erbium ions  $^4I_{15/2} - ^4I_{13/2}$  is interesting because the wavelength of this transition  $\lambda = 1536\text{ nm}$  lies in the transparency window of a standard telecommunication fiber. The coherence time of this optical transition reaches 1.4 ms in an external magnetic field for the lifetime of the excited optical state  $T_1 \sim 14\text{ ms}$  and the inhomogeneous broadening of the transition 500 MHz [19,20]. The presence of hyperfine sublevels  $^{167}\text{Er}^{3+}$  also allows to realize a long-lived QM on ion spin states, where the coherence time between spin states can reach 1 s, as was shown in [21]. Additionally, experiments were carried out to conserve light fields with a small number of photons. In this case, the input pulse contained on average of 68 photons, and the revival of silenced echo signal was — approximately one photon. The quantum noise caused by the residual excitation of atoms in the excited state in the time echo mode ( $2.2\mu\text{s}$ ) was 0.24 photons.

Next, the dependence of the efficiency of the revival of silenced echo recovery on the intensity of the rephasing pulses was studied. The results of measuring the recovery efficiency of the input pulse are shown in Fig. 4, a. Despite the use of rephasing pulses with amplitude and frequency modulation, with an increase in the intensity of such pulses, the efficiency of recovery of the input signal decreased (black squares in Fig. 4, b). This can be explained by the effect of instantaneous spectral diffusion [22,23]. This conclusion confirms the fact that the coherence time of the optical transition decreases with increasing intensity of the rephasing pulses (red circles in Fig. 4, b), which explains the decrease in the input pulse recovery efficiency in the implemented ROSE protocol.

In the present work, we fabricated waveguide structures of the third type in a Tm:YAG crystal using the femtosecond laser printing method. The advantage of such structures is that radiation with arbitrary light polarization can propagate in them. Moreover, in the paper [24] it was shown that in this crystal it is also possible to create waveguide beam splitters  $2 \times 2$  and  $3 \times 3$  with different power division ratios, which allows to manufacture an optical chip with a given logic on a single chip. In the manufactured single-mode waveguide structure in a Tm:YAG crystal, the optical QM protocol was implemented for the first time in a revival of silenced echo scheme. The recovery efficiency of input pulse was 0.5% for a storage time of  $30\mu\text{s}$ . Storage of coherent optical pulses, attenuated to an average of one photon, was achieved for a signal-to-noise ratio of  $\sim 4$  in the revival of silenced echo signal. The effects of instantaneous spectral diffusion led to the fact that, despite the use of rephasing pulses with amplitude and frequency modulation, the recovery efficiency decreased with increasing pulse

intensity. It should be noted that the effect of instantaneous spectral diffusion is more than an order of magnitude weaker in the  $\text{Tm}^{3+}:\text{Y}_3\text{Ga}_5\text{O}_{12}$  (YGG) [22] crystal. The optical transition of thulium ions in this crystal has a longer coherence time [25,26], which will also allow to increase the recovery efficiency of the revival of silenced echo signal, and, consequently, to increase the signal-to-noise ratio in the echo signal when working with single-photon light fields.

### Funding

The study was supported by the Ministry of Science and Higher Education of the Russian Federation (Register № NIOKTR 121020400113-1). S.P. Kulik thanks the Ministry of Science and Higher Education of the Russian Federation on the basis of FSAEI HE „SUSU (NRU)“ (agreement № 075-15-2022-1116 dated 01.07.2022)

### Conflict of interest

The authors declare that they have no conflict of interest.

### References

- [1] J.-H. Kim, S. Aghaieimibodi, J. Carolan, D. Englund, E. Waks. *Optica*, **7**, 291 (2020).
- [2] N. Sangouard, C. Simon, H. de Riedmatten, N. Gisin. *Rev. Mod. Phys.*, **83**, 33 (2011).
- [3] F. Kaneda, F. Xu, J. Chapman, P.G. Kwiat. *Optica*, **4**, 1034 (2017).
- [4] F. Bussi eres, N. Sangouard, M. Afzelius, H. De Riedmatten, W. Tittel. *J. Mod. Opt.*, **60**, 1519 (2013).
- [5] G. Corrielli, A. Seri, M. Mazzera, R. Osellame, H. de Riedmatten. *Phys. Rev. Appl.*, **5**, 054013 (2016).
- [6] C. Liu et al. *Optica*, **7**, 192 (2020).
- [7] A. Seri, G. Corrielli, D. Lago-Rivera, A. Lenhard, H. de Riedmatten, R. Osellame, M. Mazzera. *Optica*, **5**, 934 (2018).
- [8] C. Liu, T.X. Zhu, M.X. Su, Y.Z. Ma, Z.Q. Zhou, C.F. Li, G.C. Guo. *Phys. Rev. Lett.*, **125**, 260504 (2020).
- [9] A. Seri, D. Lago-Rivera, A. Lenhard, G. Corrielli, R. Osellame, M. Mazzera, H. De Riedmatten. *Phys. Rev. Lett.*, **123**, 80502 (2019).
- [10] M. Afzelius, C. Simon, H. De Riedmatten, N. Gisin. *Phys. Rev. A*, **79**, 052329 (2009).
- [11] V. Damon, M. Bonarota, A. Louchet-Chauvet, T. Chaneli ere, J.-L. Le Gou et. *New J. Phys.*, **13**, 093031 (2011).
- [12] M.M. Minnegaliev, K.I. Gerasimov, R.V. Urmancheev, A.M. Zheltikov, S.A. Moiseev. *Phys. Rev. B*, **103**, 174110 (2021).
- [13] M.M. Minnegaliev, K.I. Gerasimov, T.N. Sabirov, R.V. Urmancheev, S.A. Moiseev. *JETP Lett.*, **115**, 720 (2022).
- [14] F. Chen, J.R.V. de Aldana. *Laser Photon. Rev.*, **8**, 251 (2014).
- [15] M.M. Minnegaliev, I.V. Dyakonov, K.I. Gerasimov, A.A. Kalinkin, S.P. Kulik, S.A. Moiseev, M. Yu Saygin, R.V. Urmancheev. *Laser Phys. Lett.*, **15**, 045207 (2018).
- [16] M.N. Popova, E.P. Chukalina, S.A. Klimin, M.-C. Chou. *Quantum Electron.*, **50**, 256 (2020).
- [17] L. Veissier, C.W. Thiel, T. Lutz, P.E. Barclay, W. Tittel, R.L. Cone. *Phys. Rev. B*, **94**, 1 (2016).
- [18] C.W. Thiel, T. B ottger, R.L. Cone. *J. Lumin.*, **131**, 353 (2011).
- [19] R.M. Macfarlane. *J. Lumin.*, **100**, 1 (2002).
- [20] T. B ottger. *Laser Frequency Stabilization to Spectral Hole Burning Frequency References in Erbium-Doped Crystals: Material and Device Optimization* (Montana State University, 2002).
- [21] M. Ran ci , M.P. Hedges, R.L. Ahlefeldt, M.J. Sellars. *Nat. Phys.*, **14**, 50 (2017).
- [22] C.W. Thiel, R.M. Macfarlane, Y. Sun, T. B ottger, N. Sinclair, W. Tittel, R.L. Cone. *Laser Phys.*, **24**, 106002 (2014).
- [23] J. Dajczgewand, R. Ahlefeldt, T. B ottger, A. Louchet-Chauvet, J.L. Le Gou et, T. Chaneli ere. *New J. Phys.*, **17**, 23031 (2015).
- [24] N. Skryabin, A. Kalinkin, I. Dyakonov, S. Kulik. *Micromachines*, **11**, 1 (2020).
- [25] C.W. Thiel, N. Sinclair, W. Tittel, R.L. Cone. *Phys. Rev. Lett.*, **113**, 160501 (2014).
- [26] M.F. Askarani et al. *Phys. Rev. Lett.*, **127**, 220502 (2021).

*Translated by E.Potapova*